How to smooth diffusion tensor images in a voxel based analysis?

W. Van Hecke[1], A. Leemans[2], S. De Backer[1], P. M. Parizel[3], and J. Sijbers[1]

[1]University Antwerp, Antwerp, Antwerp, Belgium, [2]CUBRIC, University of Cardiff, Cardiff, Wales, United Kingdom, [3]Radiology, Antwerp University Hospital, Antwerp, Antwerp, Belgium

Introduction: Many DTI studies are starting to use voxel based analysis (VBA) to evaluate differences in the diffusion properties between healthy diseased subjects. Despite the intuitively appealing approach of analyzing diffusion measures at each voxel, VBA results should be interpreted cautiously, since they depend on the applied parameter settings. Since, for example, in the VBA literature of DTI data sets, a large range of isotropic smoothing kernel widths from 0 mm to as much as 16 mm is used, the VBA results are less standardized than they promised to be, especially since Jones et al. demonstrated that the VBA results depend on the applied smoothing kernel width (1-3). Smoothing is performed in a VBA setting to increase the sensitivity of the pathology detection, following the matched filter theorem, and to mitigate the effect of coregistration errors. In this context, a smoothing kernel width that corresponds to the expected size and shape of the pathology should be applied. In this work, simulated DTI data sets with a predefined pathology are used to evaluate the sensitivity and specificity of the VBA pathology detection comparing isotropic and anisotropic smoothing kernels with different full width at half maximum (FWHM).

Methods: Simulated DTI data sets are constructed with a specific pathology as defined by a predefined location, extent, and level of tissue degradation. The method can be summarized as follows: (a) 40 DTI data sets are acquired on a 1.5T scanner ($2x2x2mm^3$). (b) All 40 DTI data sets are transformed to the Montreal MNI space with an affine transformation based on the FA maps (c) A population specific atlas is constructed from these images in MNI space (4). (d) The resulting atlas is regarded as the fundamental image and is copied 40 times. (e) In half of these atlases, the diffusion properties are altered to introduce a pathology in a predefined number of voxels: i.e., the transverse diffusivity is increased by six different corresponding with an FA decrease of 7%, 10%, 13%, 16%, 19%, and 22%. (f) Inter-subject variability of the diffusion properties is introduced in all atlas images, i.e. in the 20 original atlases and in the 20 atlases with a pathology. (g) Finally, a realistic amount of Rician noise is added to the data sets. The FA maps of these data sets are subsequently smoothed before a non-parametric Mann-Whitney U test is performed in each voxel. In this work, the false discovery rate method of Benjamini and Hochberg was used to correct the p-values for multiple comparisons. A false discovery rate bound of p=0.05 was thereby applied. To evaluate the effect of the isotropic smoothing kernel size on the sensitivity and the specificity of the VBA analysis, the data sets are smoothed with smoothing kernels of different FWHM: 3 mm, 6 mm, 9 mm, and 12 mm. An edge and corner preserving filter for magnitude MR data was constructed using an anisotropic Gaussian smoothing kernel shaped by the eigenvalues and eigenvectors of a local gradient tensor and applied to the FA maps (5). Analogously as in the isotropic smoothing approach, the effect of the smoothing kernel width on the VBA results is evaluated by smoothing the data sets with a similar range of FWHMs: 3 mm, 6 mm, 9 mm, and 12 mm.

Results: The effect of isotropic and anisotropic smoothing on an FA image is visualized for a random axial slice in Fig. 1 for different isotropic and anisotropic smoothing kernels with a FWHM ranging from 0 mm to 12 mm. The validity of the matched filter theorem is analyzed using the simulated data sets in Fig. 2. To this end, the FWHM that produced the highest sensitivity to detect a certain pathology is mapped against the size of this pathology. This is done for different levels of pathology, corresponding with an FA decrease of 10%, 13%, 16%, and 19%. A significant correlation is found between the optimal FWHM and the size of the pathologies when the data sets were smoothed with an anisotropic kernel ($p<0.05$ using the Spearman correlation test) and no correlation was found for the isotropic smoothing approach ($p>>0.05$). The sensitivity and the specificity of the VBA results are displayed in a receiver-operating characteristic (ROC) plot in Fig. 3 for the different smoothing approaches, various kernel widths, and different levels of pathology, displaying the true positive rate (=sensitivity) as a function of the false positive rate (=100-specificity). In Fig. 4, VBA results are displayed on 10 axial slices for both smoothing approaches and different smoothing kernel widths. A level of pathology corresponding with an FA decrease of 19% was thereby introduced. The voxels that contain a ground truth pathology are colored in green, whereas the VBA results are colored in red. Consequently, the voxels in which the VBA results and the ground truth overlap are colored in yellow. A green, red, and yellow color thus represents the presence of false negative, false positive, and true positive results, respectively. Voxels in which the background FA values are displayed correspond with true negative results.

Conclusion: Our results based on simulated DTI data sets indicate that the sensitivity as well as the specificity of the pathology detection are significantly reduced when the data sets are smoothed isotropically with a FWHM larger than 3 mm in a VBA study. Using simulated DTI data sets, we demonstrated that the use of anisotropic smoothing kernels can significantly increase the sensitivity and the specificity of detecting a pathology in a VBA study. We therefore suggest to apply an anisotropic smoothing method in DTI group studies to increase the SNR while preserving WM boundaries.

Ref:[1]Jones et al,2005,NeuroImage;[2]Borroni et al,2007,Arch Neurol;[3]Sage et al,2007,NeuroImage;[4]Van Hecke et al,2007,NeuroImage;[5]Sijbers etal,1999, MRI

Fig. 1

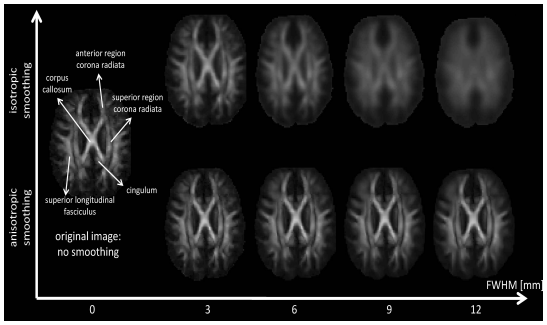

Fig. 2

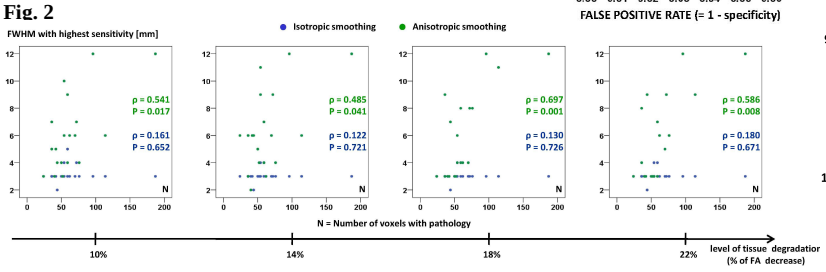

Fig. 3

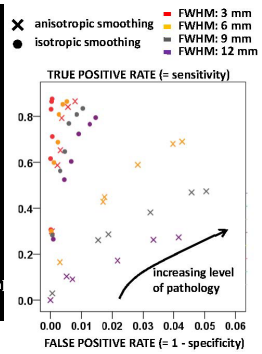

Fig. 4